Manufacturing of screw rotors via 5-axis double-flank CNC machining

Michal Bizzarri[a,*], Michael Bartoň[a,b]

[a] *BCAM – Basque Center for Applied Mathematics, Alameda de Mazarredo 14, 48009 Bilbao, Basque Country, Spain*
[b] *Ikerbasque – Basque Foundation for Sciences, Maria Diaz de Haro 3, 48013 Bilbao, Basque Country, Spain*

Abstract

We investigate a recently introduced methodology for 5-axis flank computer numerically controlled (CNC) machining, called *double-flank* milling [1]. We show that screw rotors are well suited for this manufacturing approach where the milling tool possesses tangential contact with the material block on two sides, yielding a more efficient variant of traditional flank milling. While the tool's motion is determined as a helical motion, the shape of the tool and its orientation with respect to the helical axis are unknowns in our optimization-based approach. We demonstrate our approach on several rotor benchmark examples where the pairs of envelopes of a custom-shaped tool meet high machining accuracy.

Keywords: 5-axis CNC machining, double-flank milling, custom-shaped tool, screw rotor

1. Introduction & Motivation

Efficient and highly-accurate manufacturing of curved geometries such as car transmissions, gearboxes, screw rotors, and other doubly-curved engine parts is a considerable challenge in many industries like automotive or aeronautic, to name a few. *Screw compressors* are engine components used to compress gas, cf. [2].

Figure 1: Screw compressor rotors. Male (left) and female (right) parts.

It is a positive displacement machine provided with two parallel helical rotors, a *male rotor* and a *female rotor*, which are engaged one with the other as they rotate, cf. Fig. 1. The interaction preserves tangential contact that, due to the helical nature of both parts, is achieved along a helix. This contact helix changes over time which results that the fluid/gas confined in the cavities is being transferred in the axial direction. The geometry of screw rotors may vary depending on the number of *lobes* in each rotor, the basic *rotor profile*, and relative proportions of each rotor lobe segment, however, geometrically the boundaries of screw rotors are always helical surfaces.

Manufacturing of screw rotors is a complex process that typically requires a special type tool and/or machine [3, 4]. Such a machine is expensive and our approach focuses on manufacturing using a traditional machining centers via 5-axis computer numerically controlled (CNC) machining. Our research aims at the final stage of machining, called *flank*, where the tool touches the reference surface along a whole curve. In this stage of machining, high accuracy of a few micrometers for objects of size of tens of centimeters is required.

We further explore a recently-introduced variant of flank milling, called *double-flank* milling, where the tool has tangential contact with the material on two sides of the tool. It has been shown recently that one such a suitable geometry that admits double-flank milling within high manufacturing tolerances is the "valley" between teeth of a spiral bevel gear [1]. In this work, we further explore this methodology and show that most of the existing parts, both male and female, of screw rotors can be double-flank milled with an appropriate custom-shaped tool within fine machining tolerances. For screw rotors that arise from symmetric planar profiles, we show that the double-machining is theoretically exact, and for non-symmetric rotors we propose an optimization-based framework that computes the tool's shape and position.

*Corresponding author
Email addresses: mbizzarri@bcamath.org (Michal Bizzarri), mbarton@bcamath.org (Michael Bartoň)

The rest of the paper is organized as follows. We overview related research on screw rotors design and manufacturing in Section 2. Approximation of screw rotors with symmetric profiles is discussed in Section 3 and the asymmetric case in Section 4. Double-flank machining with conical tools is addressed in Section 5 and the conclusions are drawn in Section 6.

2. Previous Work

Regarding the design stage, one can find various shapes of screw rotors, see e.g. [3–6] and many other relevant references cited therein, see Fig. 2. A frequently used approach is to design one part (male or female) and consider its relative motion with respect to the other, yet unknown part. This boils down to a 2D gearing problem. The other part is then defined as an envelope of the one-parameter family of positions of the first part under a cycloidal motion [4]. This approach has also been used recently for design of 2D gears [7]. For two given 2D shapes to form a pair of non-circular gears, an optimization-based framework that looks for position of rotational centers that admit gearing configuration is presented in [8].

While the geometry of a smooth transition between the male and female rotor is the main objective in the design stage, one has to keep in mind that the rotors serve as fluid pumps and therefore their performance is affected by a lot of physics. Another class of relevant research deals with computational fluid dynamics and optimizes the shape of rotors to comfort the flow of the fluid under consideration [9, 10]. Pressure and fluid velocity is simulated and the rotor profile is optimized towards better gas compression performance [10].

Approximation of helical surfaces using traditional cutters with straight (cone, cylinder) and circular (sphere, torus) profiles is a well-studied problem [11]. One can analyse the second order behavior of the tool and the surface and find locally best position of the helical surface and the cutter. Such an analysis, however, finds a good match only at a contact point, and due to the helical nature of the surface, along a helix. The approximation quality naturally decreases for points farther away from the helix. In the context of manufacturing, one needs many passes of the tool to get the desired accuracy. In contrast, our approach looks for tangential contact along a whole curve (on the cutter) such that the pair of helical surfaces can be milled, ideally, with a single pass.

Manufacturing of screw rotors is typically achieved using a special helical grinding machines, similarly to the manufacturing of curved gears [12, 13]. Such an approach, however, is very expensive as the machine is designed specifically for the gears/rotors and is therefore meant for large manufacturing batches. Therefore, the design of the shape of the rotors is typically linked with a specific hobbing tool [14]. In contrast, our research aims at manufacturing screw rotors in standard 5-axis milling centers, that can be used e.g. for manufacturing of a single piece

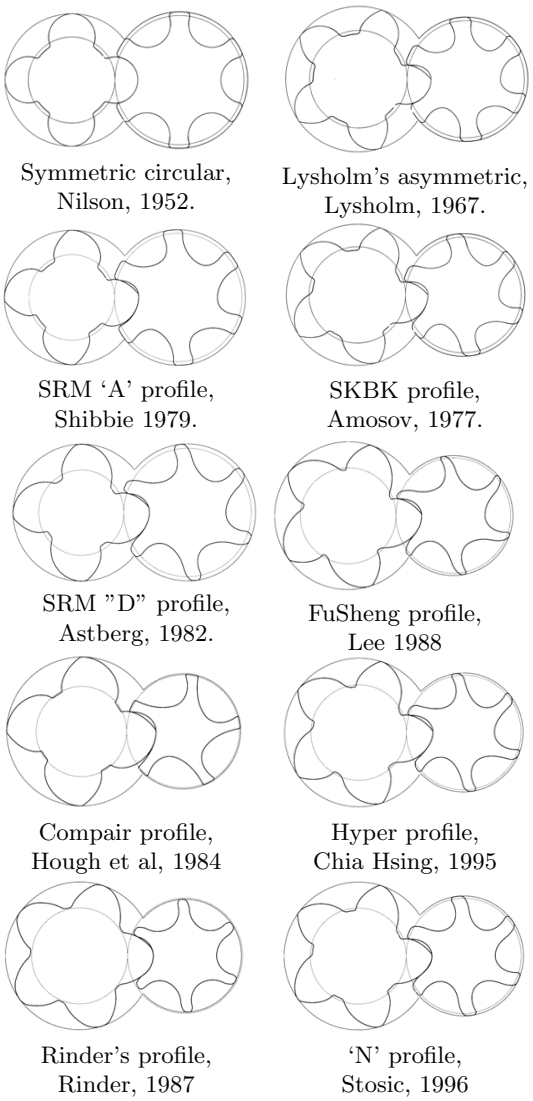

Figure 2: Most popular screw compressor rotor profiles today [2].

(e.g. a replacement of a broken part). To reach a high machining quality, we follow the recent trend and look for a custom-shaped tool that admits higher approximation quality than on-market conical and cylindrical tools, typical for flank milling [1].

An alternative approach of screw rotor manufacturing is using molds, via so-called resin transfer molding (RTM)[15]. The molds are filled by carbon composite and clamped to form the desired object. This approach, however, assumes to have sufficiently accurate complement of the objects, i.e., the mold, and therefore the problem accurate workpiece is transferred to manufacturing the mold.

Inspired by mold design or support structures of modern free-form architecture, there is a broad literature on approximation of curved (free-form) surfaces using motions of simple geometric objects as straight lines and/or circular arcs [16–18]. In this class of research, one aims to approximate a curved input surface by motions of simple

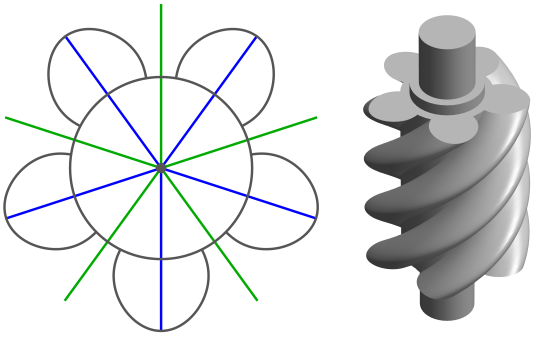

Figure 3: Symmetric profile with five lobes – all lobes are symmetric with respect to the blue axes. The gaps between the lobes are symmetric w.r.t. the green axes.

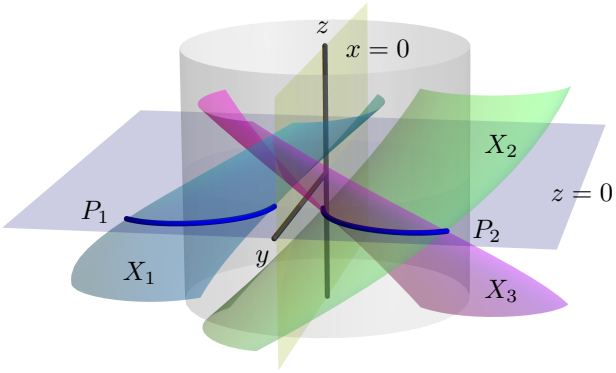

Figure 4: Symmetry of helical surfaces. Two helical surfaces X_1 and X_2, that are generated by screwing two mutually symmetric planar profiles P_1 and P_2, can be rigidly mapped one onto another via two planar symmetries.

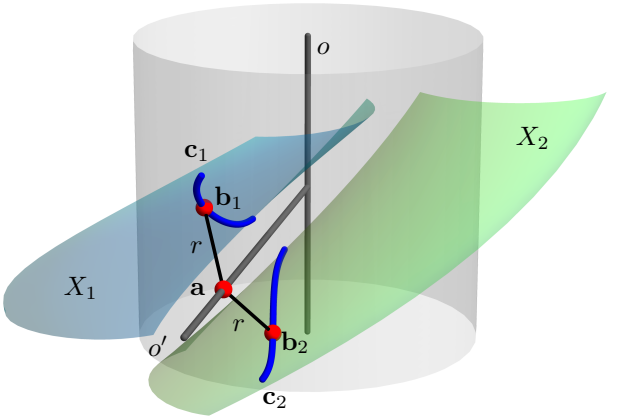

Figure 5: Characteristics $\mathbf{c}_1$ and $\mathbf{c}_2$ on the two symmetric helical surfaces X_1 and X_2.

objects, these being either given as input or unknowns. The motion of the simple object is an unknown and there are additional constraints on the motions such as fairness or rigidity, in the case of dynamic linkages [19]. Our optimization approach differs as the motion is given and we are looking for the shape of the tool.

3. The screw rotors with symmetric profiles

The body of a helical rotor is obtained by applying a screw motion to a planar profile. The screw motion is defined by its *axis* o, typically perpendicular to the plane of the profile, the *handedness* (it can be right-handed or left-handed) and the value of the *pitch* $2\pi v_0$. In particular the right-handed helical surface given by the planar profile curve $\mathbf{p}(u) = (p_1(u), p_2(u))$ and the pitch $2\pi v_0$ has the form

$$\mathbf{x}(u,v) = (p_1(u)\cos(v) - p_2(u)\sin(v), \\ p_1(u)\sin(v) + p_2(u)\cos(v), v_0 v)\,. \quad (1)$$

Consider a screw rotor with a *symmetric* profile, i.e., each lobe is symmetrical w.r.t. its axis, see the blue axes in Fig. 3 (left). Hence the gaps between the lobes are also symmetric, cf. the green axes in Fig. 3 (left). We show, that in such case the screw rotor can be double-flank milled exactly. We also design the exact shape of the tool.

Proposition 3.1. *Two helical (screw) surfaces X_1 and X_2 generated by screwing two planar symmetric curves P_1 and P_2 with the axis of the symmetry o' passing through the axis o of the screw are symmetrical w.r.t. o'.*

Proof. W.l.o.g we identify o and o' with the z- and y-axis, respectively. Let X_3 be a reflection of X_1 through the plane $x = 0$. Since the reflection through the plane changes the handedness, X_3 is just screwed surface generated by screwing P_2 in the opposite handedness, see Fig. 4. X_3 is simultaneously a reflection of X_2 through the plane $z = 0$. Composing these two plane reflections yields reflection through the axis $y = 0$. □

Corollary 3.2. *The screw rotors with symmetric profiles can be double-flank milled exactly.*

That is, the symmetry of the planar profile admits a *general* rotational tool that is tangential to both X_1 and X_2. The construction of the rotational tool is as follows. To flank mill a helical surface, the trajectory of the tool's axis is a ruled helical surface. For symmetric profile, the tool axis o' is perpendicular to o and the trajectory is a helicoid. The tool is a rotational surface that can be seen as an envelope of one parameter family of spheres centered at o'. To describe the shape of the tool, one has to know its radial function $r(u)$. Hence for all points $\mathbf{a}$ of the axis o' we compute the so called *foot points* $\mathbf{b}_1$ on X_1, where the foot point $\mathbf{b}$ of a point $\mathbf{a}$ on a surface X is defined as a point on X with the minimal distance from $\mathbf{a}$, i.e., $\mathbf{b} = \mathbf{x}(u_0, v_0)$, where the following conditions hold

$$\begin{aligned} (\mathbf{x}(u_0,v_0) - \mathbf{a}) \cdot \left.\frac{\partial \mathbf{x}(u,v)}{\partial u}\right|_{u=u_0,v=v_0} &= 0, \\ (\mathbf{x}(u_0,v_0) - \mathbf{a}) \cdot \left.\frac{\partial \mathbf{x}(u,v)}{\partial v}\right|_{u=u_0,v=v_0} &= 0. \end{aligned} \quad (2)$$

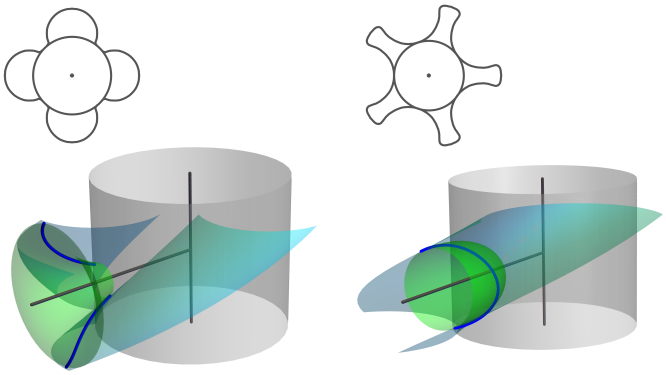

Figure 6: Design of the ideal tool for double-flank milling of the male (left) and female (right) helical rotor with the symmetric profiles (Nielson, 1952) from Example 3.3. The tools match exactly the valleys between the lobbes.

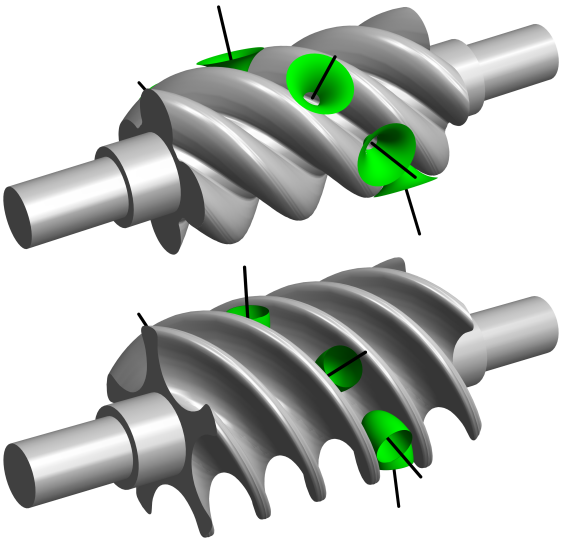

Figure 7: Exact double-flank milling of male (up) and female (bottom) screw rotors with symmetric profiles (Nielson, 1952) from Example 3.3. Several positions of the custom-shaped tools are shown.

The foot points $\mathbf{b}_1$ are symmetrical to foot points $\mathbf{b}_2$ on X_2 through o'. Finally the radial function is given by $r = \|\mathbf{a} - \mathbf{b}_1\| = \|\mathbf{a} - \mathbf{b}_2\|$, see Fig. 5.

More precisely when points on o' are given by $(0, \lambda, 0), \lambda \in [\lambda_0, \lambda_1]$ and the profile curve P_1 by $\mathbf{p}(u)$, we solve (for each value of $\lambda \in [\lambda_0, \lambda_1]$) Eq. (2), i.e.,

$$\begin{aligned} (\lambda(\sin v, \cos v) - \mathbf{p}(u)) \cdot \mathbf{p}'(u) &= 0, \\ \lambda(\cos v, -\sin v) \cdot \mathbf{p}(u) - v_0^2 v &= 0, \end{aligned} \tag{3}$$

which yields the corresponding foot points $\mathbf{b}_1 \in X_1$ and consequently $r(u)$.

Example 3.3 (Nilson, 1952)**.** The first screw male rotor profile ever generated is defined by the symmetric profile consisting of four circular arcs, see Fig. 6.

This symmetric profile has a huge blow-hole area which excludes it from any compressor application where a high

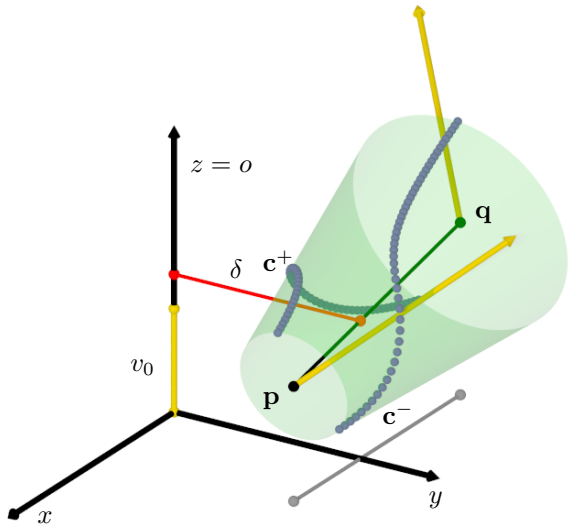

Figure 8: A right-handed screw motion with the axis $o \equiv z$ and a reduced pitch v_0 is applied to a truncated cone with axis $o' = \mathbf{pq}$. The position of o' w.r.t o is controlled by two parameters: the distance $\delta = \text{dist}(o, o')$ (red) and α that controls the slope. Here $\alpha = 0.2$; $\alpha = 0$ corresponds to the case when o' is parallel to its orthogonal projection (gray) to the xy-plane. The instantaneous velocity vectors at the axis endpoints (yellow) are tangent to the helices passing through $\mathbf{p}$ and $\mathbf{q}$ and the characteristics $\mathbf{c}^{\pm}$ are shown in blue.

or even moderate pressure ratio is involved. However, the symmetric profile performs surprisingly well in low pressure compressor applications [2]. The design of the exact tools and the milling process of those symmetric screw rotors is shown in Figs. 6 and 7.

4. The screw rotors with asymmetric profiles

Most of the rotors are asymmetric, see Fig. 2, and these rotors, in general, cannot be double-flank milled exactly. One can obviously consider only a (single-)flank milling and design two custom-shaped tools and apply two milling paths, each for every helical surface. However, the challenge that we aim to address in this work is whether it is possible to approximate the tool and the path sufficiently accurate with a single tool and a single path.

Due to the helical shape of the surfaces to be milled, it is natural to constraint the motion of the tool as the corresponding helical motion. We therefore look for the position of the axis o' with respect to o and the radial function $r(u)$.

Remark 4.1. While in the context of CNC machining 5-axis machines are the most flexible ones, and therefore can be used for our purpose, geometrically we do not need that many degrees of freedom. Since the motion is helical, the tool does not change its position with respect to the helical axis of the rotor. Only two degrees of freedom are needed, one controlling the rotation and the other the translation of the rotor.

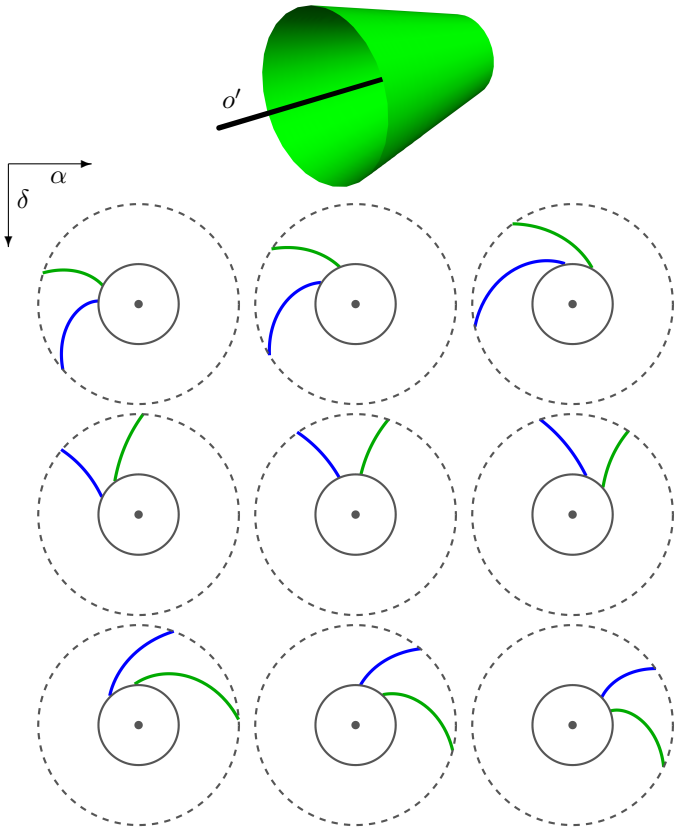

Figure 9: Design of double-flank millable profiles. Given a conical tool T (top), position of its axis o' with respect to the screw axis is controlled using a pair of parameters (α, δ). Here $\alpha = -0.7, 0, 0.7$ from left to right and $\delta = -0.7, 0, 0.7$ from top to bottom. Depending on their values, the planar profiles that admit exact double-flank milling with T are computed via Eq. (8).

4.1. Modeling of double-flank millable surfaces

Let the right-handed screw be given by its axis o, without loss of generality we assume $o \equiv z$, and its screw pitch $2\pi v_0$, see Fig. 8. We start our approach by considering all possible profiles of helical surfaces which can be exactly double-flank milled by a free-form tool T. Let T be given by its axis o' in generic position

$$o' : (\delta, u, u\tan(\alpha)), \quad u \in [u_0, u_1], \tag{4}$$

where u is the parameter of the parameterization of o' and δ and α correspond to the position of o', i.e., the line o' has a direction $(0, 1, \tan(\alpha))$ (it possesses the angle α with the plane $z = 0$) and goes through the point $(\delta, 0, 0)$ (it has a distance δ from o).

Let $r(u)$ be the radial function that determines T.

We proceed with the computation of the characteristic $\mathbf{c}^{\pm}$ on T as follows: Screwing o' and appending the radial function $r(u)$ yields the Medial Surface Transform (MST)

$$\begin{aligned}\overline{\mathbf{y}}(u,v) = (\mathbf{y}(u,v), r(u)) = (\delta\cos(v) - u\sin(v),\\ u\cos(v) + \delta\sin(v), u\tan(\alpha) + vv_0, r(u))\,.\end{aligned} \tag{5}$$

Employing the envelope formula, see e.g. Eq. (4) in [20], yields the so called *characteristic*, i.e., the curve along which the moving tool T touches its envelope. Thus, the two branches of the characteristic have the following parameterization

$$\begin{aligned}\mathbf{c}^{\pm} = \frac{1}{EG - F^2}\,(\mathbf{y}_1(r_1G - r_2F) + \mathbf{y}_2(r_2E - r_1F) \pm\\ (\mathbf{y}_1 \times \mathbf{y}_2)\sqrt{(E - r_1^2)\,(G - r_2^2) - (F - r_1r_2)}\Big)\,,\end{aligned} \tag{6}$$

where

$$\begin{aligned}(\mathbf{y}_1, r_1) &= \left.\frac{\partial\overline{\mathbf{y}}(u,v)}{\partial u}\right|_{v=0} = (0, 1, \tan(\alpha), r'(u)),\\ (\mathbf{y}_2, r_2) &= \left.\frac{\partial\overline{\mathbf{y}}(u,v)}{\partial v}\right|_{v=0} = (-u, \delta, v_0, 0)\end{aligned} \tag{7}$$

and $E = \mathbf{y}_1\cdot\mathbf{y}_1$, $F = \mathbf{y}_1\cdot\mathbf{y}_2$, $G = \mathbf{y}_2\cdot\mathbf{y}_2$. Then by screwing characteristic $\mathbf{c}^{\pm} = (c_1^{\pm}, c_2^{\pm}, c_3^{\pm})$ to the plane $z = 0$ we arrive at the planar profile

$$\begin{aligned}\mathbf{h}^{\pm} = \left(c_2^{\pm}\sin\left(\varphi^{\pm}\right) + c_1^{\pm}\cos\left(\varphi^{\pm}\right),\right.\\ \left. c_1^{\pm}\sin\left(\varphi^{\pm}\right) + c_2^{\pm}\cos\left(\varphi^{\pm}\right)\right)\,,\end{aligned} \tag{8}$$

where

$$\varphi^{\pm} = -\frac{c_3^{\pm}}{v_0}. \tag{9}$$

This approach can be used directly for modeling a pair of helical surfaces which can be exactly double-flank milled by a given tool, see Fig. 9. It is a direct problem where the shape of the tool directly determines a pair of its envelopes.

However, we are interested in the more difficult inverse problem, where the shape of the rotor is given and one looks for a proper tool T and its position to approximate it within high accuracy on both sides of the tool, that is, to find a double-flank configuration. We achieve that using optimization approach by minimizing the distance between a given asymmetric profile and a free-form tool (8).

4.2. Double-flank milling with custom-shaped tools

Now, we describe an approach for computing the ideal position of o' and radial function r based on minimizing the differences between the distance of o' and characteristics $\mathbf{c}^{\pm}$.

In particular, for a given position of the axis o' we compute the foot points $\mathbf{b}_1^i$ and $\mathbf{b}_2^i$ of the points $\mathbf{a}_i$ sampled on the axis o'. Since we need to consider also the rotation around axis o, the axis o' is now given by

$$o' : (\delta\cos(\phi) - u\sin(\phi), u\cos(\phi) + \delta\sin(\phi), u\tan(\alpha)), \tag{10}$$

i.e., it is a rotated axis (4) around the axis z by an angle ϕ. Then we define the objective function Φ as the maximum

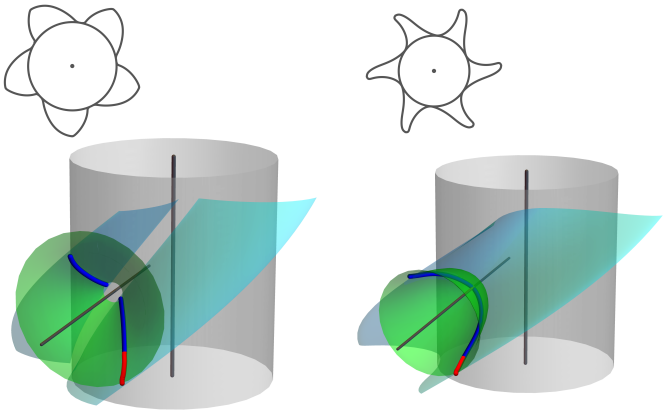

Figure 10: Design of the ideal tool for double-flank milling of the male (left) and female (right) helical rotor with the asymmetric profiles ('N' profile, Stosic, 1996) from Example 4.3.

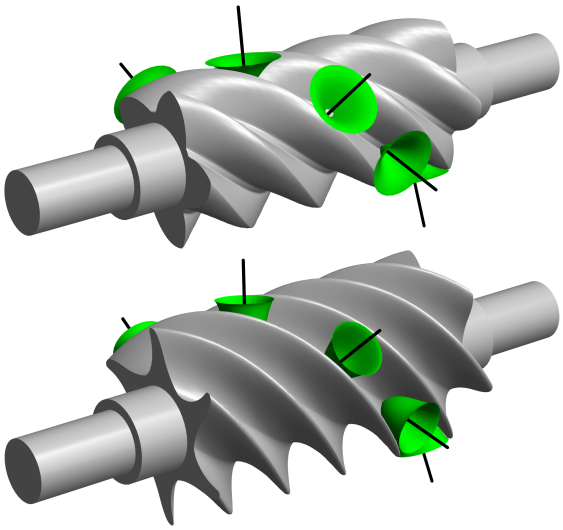

Figure 11: Approximate double-flank milling of male (up) and female (bottom) screw rotors with asymmetric profiles ('N' profile, Stosic, 1996) form Example 4.3. Several positions of the custom-shaped tools are shown.

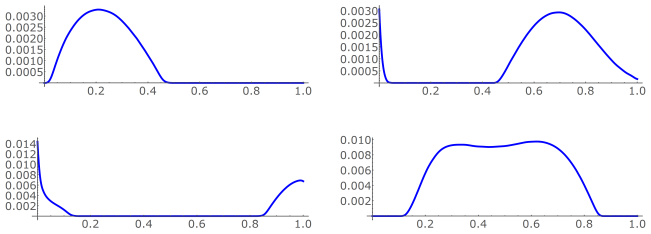

Figure 12: Error functions (15) (along the axis o') corresponding to radii (14) of the custom-shaped (male and female) tools and the helical surfaces X_1 (left) and X_2 (right) corresponding to the male (up) and female (bottom) rotors from Example 4.3.

of the differences between the distances of the foot points $\mathbf{b}_1^i$, $\mathbf{b}_2^i$ and $\mathbf{a}_i$

$$\Phi(\alpha,\delta,\phi) = \max_{i=1,\dots,n} \left| \|\mathbf{b}_1^i - \mathbf{a}_i\| - \|\mathbf{b}_2^i - \mathbf{a}_i\| \right|, \qquad (11)$$

where n is the number of samples on o'. In all our examples we choose $n = 100$ as a suitable compromise between accuracy and speed of computation. For minimizing Φ we employ the gradient descent method, where the gradient is approximated using the finite differences, i.e.,

$$\begin{aligned}\nabla\Phi(\alpha_0,\delta_0,\phi_0) \approx ((&\Phi(\alpha_0+h,\delta_0,\phi_0) - \Phi(\alpha_0-h,\delta_0,\phi_0),\\ &\Phi(\alpha_0,\delta_0+h,\phi_0) - \Phi(\alpha_0,\delta_0-h,\phi_0),\\ &\Phi(\alpha_0,\delta_0,\phi_0+h) - \Phi(\alpha_0,\delta_0,\phi_0-h)))/(2h) \qquad (12)\end{aligned}$$

for sufficiently small h. In all our examples we use $h = 10^{-3}$. When the two subsequent values in the optimization process do not differ by more than a prescribed value, i.e., $\|\mathbf{x}_{i+1} - \mathbf{x}_i\| < \varepsilon = 10^{-5}$, we stop the optimization.

Remark 4.2. The objective function (11) is not necessarily convex. Gradient descent method is used for simplicity of implementation. One can use more advanced optimization methods, such as, e.g., Levenberg-Marquardt instead. However, since the tested profiles are all close to symmetric-ones, and for those there exist an exact solution (global minimizer) as described in Section 3, it is expected that the optimized results will be similar.

This method yields a position of the tool T (its axis o') and two arrays of radii

$$r_1^i = \|\mathbf{b}_1^i - \mathbf{a}_i\|, \quad r_2^i = \|\mathbf{b}_2^i - \mathbf{a}_i\|, \qquad i = 1,\dots,n, \quad (13)$$

such that $\max|r_1^i - r_2^i|$ is minimal (and zero for symmetric screw rotors). To avoid the penetration (overcutting) we construct the radial function of T by interpolating the values

$$r^i = \min\left(r_1^i, r_2^i\right). \qquad (14)$$

The error of the approximate double-flank machining (along the axis o' of T) is measured as the distances between the tool and both sides X_1 and X_2 of the rotor, i.e.,

$$e_1^i = r_1^i - r^i, \quad \text{and} \quad e_2^i = r_2^i - r^i. \qquad (15)$$

Since the tool is moved in the same helical motion as the profile curves (and the characteristics) error functions (15) (along o') remain exactly the same during the machining process.

For a general screw rotor, the profile curves P_1 and P_2 are not symmetric (and neither X_1 nor X_2 are). It generically happens, that the characteristics $\mathbf{c}_1$ and $\mathbf{c}_2$ are not of the equal length – i.e., at some point $\mathbf{a}_k$, one of the characteristics, say $\mathbf{c}_1$, reaches the boundary of X_1 whereas $\mathbf{c}_2$ does not reach the boundary of X_2. Hence for $i > k$, we have to take care only of the foot points $\mathbf{b}_2^i$ on X_2 and the "rest" of the tool provides the exact single-flank milling of X_2, see the red curves in Fig. 10.

Example 4.3 ('N' profile, Stosic, 1996 – double-flank)**.** Since the asymmetric profiles are not far from the sym-

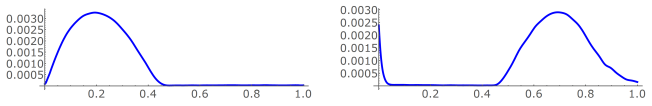

Figure 13: One-sided "rotor-to-tool" distance functions between the two parts of the male rotor and the two branches of the tool's envelope form Example 4.3. They are almost identical to the "tool-to-rotor" distance functions from Fig. 12

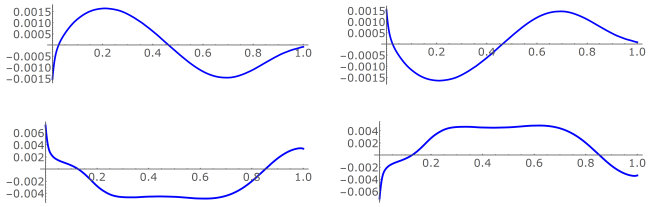

Figure 14: Error functions (15) (along the axis o') corresponding to radii (16) of the custom-shaped (male and female) tools and the helical surfaces X_1 (left) and X_2 (right) corresponding to the male (up) and female (bottom) rotors from Example 4.3.

metric ones, we use as a first guess the values $\mathbf{x}_0 = (\alpha_0, \delta_0, \phi_0) = (0, 0, 0)$. These initial values correspond to the exact solution for the symmetric profiles and therefore, by the continuity argument, one can postulate that they will serve as a good initialization for slightly non-symmetric profiles. We arrive after 18 iterations at $(\alpha, \delta, \phi) \doteq (-0.027, 0.21, 0.21)$ for the male rotor and after 24 iterations at $(\alpha, \delta, \phi) \doteq (-0.118, 0.183, 0.157)$ for the female rotor, see Figs. 10 and 11. The maximal distances between the custom-shaped tool and the surfaces X_1 and X_2 corresponding to the male rotor are less than 0.00362 and 0.00358. For the female rotor we arrive at the distances less than 0.01774, 0.01685, see Fig. 12. These values are relative to the radius $R = 1$ of the cylindrical body of both (male and female) rotors.

Remark 4.4. Considering the average of the radii

$$r^i = \frac{r_1^i + r_2^i}{2} \tag{16}$$

instead of minimum (14) allows us to lower the errors to the half. On the other hand this brings the overcutting since the errors (15) can be negative. In Fig. 14 the error functions (15) w.r.t. radial function (16) corresponding to the data from Example 4.3 are shown.

Another possibility is to define the radial function with respect to only one side of the rotor, i.e.,

$$r^i = r_1, \quad \text{or} \quad r^i = r_2, \tag{17}$$

which ensures that X_1 (or X_2) will be milled exactly whereas X_2 (or X_1) only approximately with the same maximal error as we obtain for radial function (14) but also with the possible overcutting (negative radial function). The error functions corresponding to the parts of the rotor, which are to be approximated (for the data from

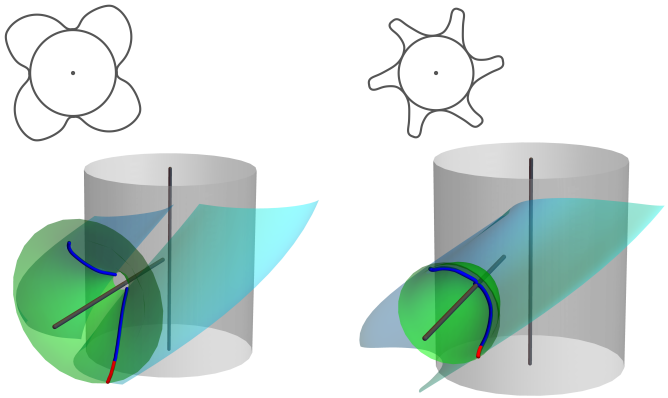

Figure 15: Design of the ideal tool for double-flank milling of the male (left) and female (right) helical rotor with the asymmetric profiles (SRM 'D' profile, Astberg, 1982) from Example 4.7.

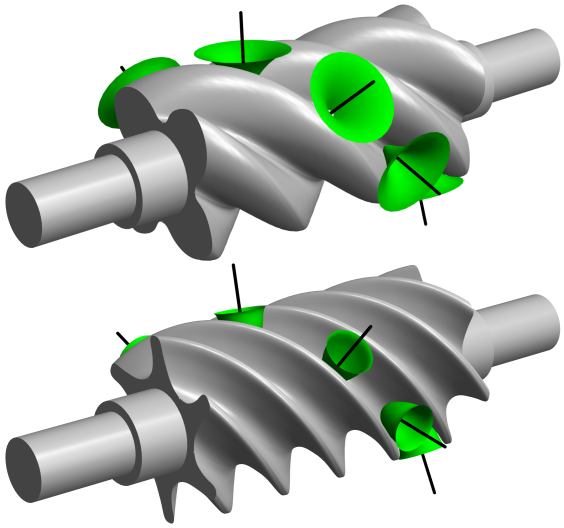

Figure 16: Approximate double-flank milling of male (up) and female (bottom) screw rotors with asymmetric profiles (SRM 'D' profile, Astberg, 1982) from Example 4.7. Several positions of the custom-shaped tools are shown.

Example 4.3) look exactly like those in Fig. 14 but with the double amplitude.

Remark 4.5. Although the proximity of two geometric entities is usually measured by the Hausdorff distance, we use, for the sake of simplicity, only the discrete approximation of the one-sided "tool-to-rotor" distance. It is very convenient since we sample points on the tool's axis and compute their footpoints on the rotor. The one-sided "rotor-to-tool" distance (the other direction) requires sampling of a curve on the rotor, e.g., the profile curve, and computing their footpoints on the envelope (created by the tool). However, our test shows that both one-sided distances are almost identical, see Example 4.6, and since the first distance is easier to compute than the second one, we use the "tool-to-rotor" distance only.

The exact computation of a Hausdorff distance requires

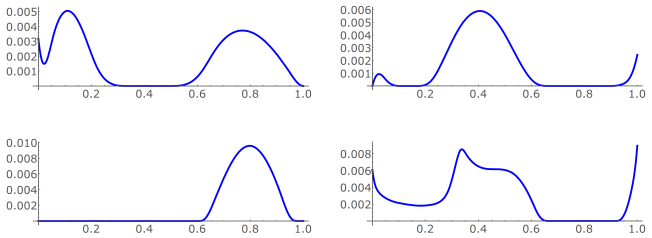

Figure 17: Error functions (15) (along the axis o') corresponding to radii (14) of the custom-shaped (male and female) tools and the helical surfaces X_1 (left) and X_2 (right) corresponding to the male (up) and female (bottom) rotors from Example 4.7.

to detect/test peculiar configurations where for instance a self bisector of one surface intersects the other surface, see e.g. [21]. However, our test surfaces (rotor and tool's envelope) are rather simple geometries and we conjecture that the Hausdorff distance occurs in the antipodal points in our case. Therefore we can approximate the Hausdorff distance by computing footpoints of a dense set of sampling points of the tool's axis.

Example 4.6. We measure the one-sided distance in the "rotor-to-tool" direction of the male rotor and the tool's envelope from Example 4.3. In particular we sample a dense set of points on two curves (different from helices) on the two sides X_1 and X_2 of the the male rotor and compute their distances to the two branches E_1 and E_2 of the envelope (created by the moving tool), see Fig. 13. Since the surfaces (rotor and tool's envelope) are rather simple geometries, both one-sided distances ("tool-to-rotor" and "rotor-to-tool") are almost identical. The discrete approximation of the Hausdorff distance is then the maximum of the maxima of both one-sided distances. In this particular example the maxima of the two one-sided distances of X_1 and E_1 are equal to 0.00362 and 0.00361. For X_2 and E_2 we arrive at 0.00358 and 0.00356. Hence the approximate Hausdorff distances between the envelope and the rotor are 0.00362 and 0.00358.

Example 4.7 (SRM 'D' profile, Astberg, 1982 – double-flank)**.** We demonstrate the designing of the custom-shape tool and finding its initial position on another standard screw rotor. We again use as a first guess the values $\mathbf{x}_0 = (\alpha_0, \delta_0, \phi_0) = (0, 0, 0)$ and employ the optimization process described above. We arrive after 24 iterations at $(-0.048, 0.089, 0.111) \doteq (-0.027, 0.21, 0.21)$ for the male rotor and after 33 iterations at $(\alpha, \delta, \phi) \doteq (-0.051, 0.29, 0.302)$ for the female rotor. The tool and its positions are shown in Figs. 15 and 16. The maximal distances between the custom-shaped tool and the surfaces X_1 and X_2 corresponding to the male rotor are less than 0.00556 and 0.00606. For the female rotor we arrive at the distances less than 0.00965 and 0.00912, see Fig. 17. These values are again relative to the radius $R = 1$ of the cylindrical body of both (male and female) rotors.

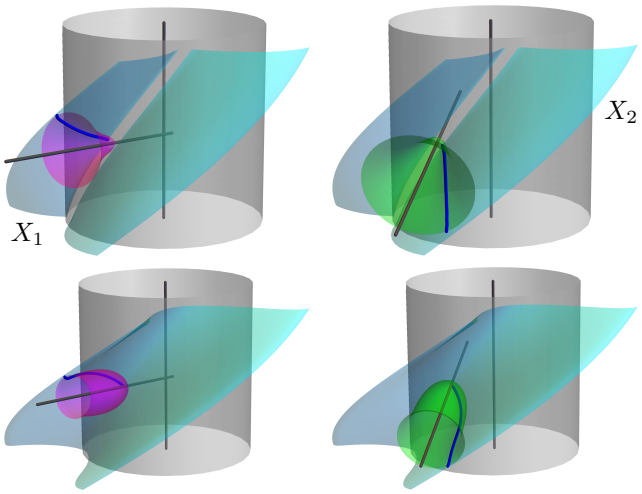

Figure 18: Design of the exact tool for single-flank milling of the male (up) and female (bottom) helical rotor with the asymmetric profiles ('N' profile, Stosic, 1996).

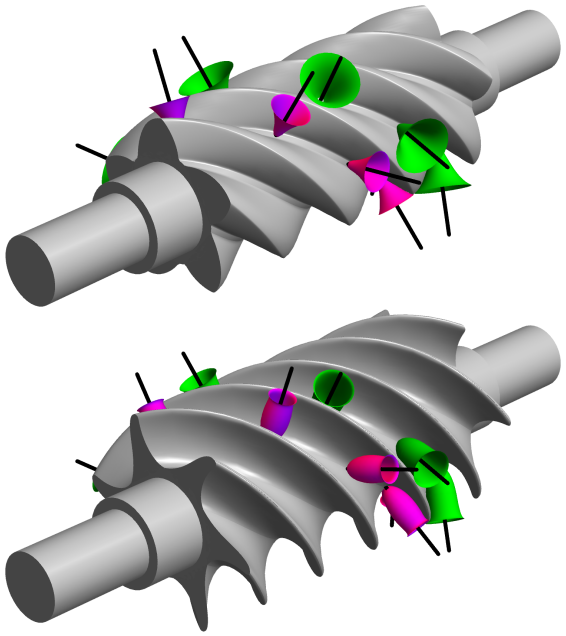

Figure 19: Exact single-flank milling of male and female screw rotors with asymmetric profiles ('N' profile, Stosic, 1996). One side of the valley of the helical rotors is exactly milled by the magenta tool whereas the other one by the green tool. Several positions of the custom-shaped tools are shown.

Remark 4.8. We have shown two examples where the double-flank milling of male components meets high accuracy requirements. For highly non-symmetric rotors, one cannot guarantee fine errors as double-flank milling is not theoretically exact for these shapes. However, one can always finish the process by single-flank milling as follows. It is enough to choose an axis o' of the tool T (almost) arbitrarily. Only, it has to be satisfied that the distance of o' to the surface X_1 which we want to mill is less than the distance to X_2. The shape of the custom-shaped tool

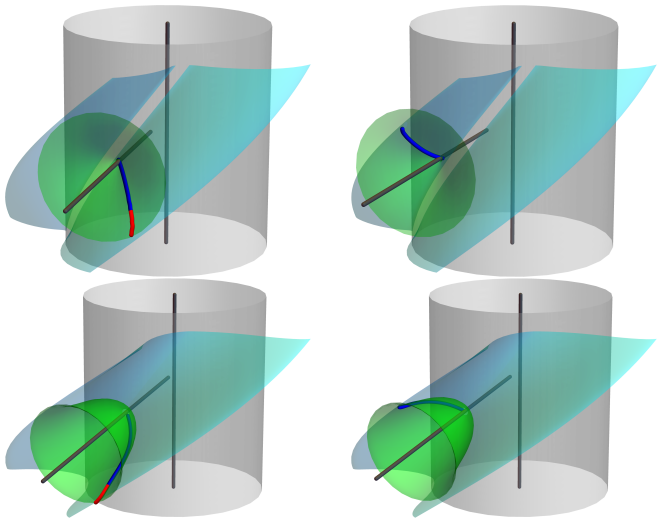

Figure 20: Design of the custom-shape tool for the approximate single-flank milling with the same tool of two helical surfaces (left and right) of male (top) and female (bottom) screw rotors ('N' profile, Stosic, 1996) from Example 4.9.

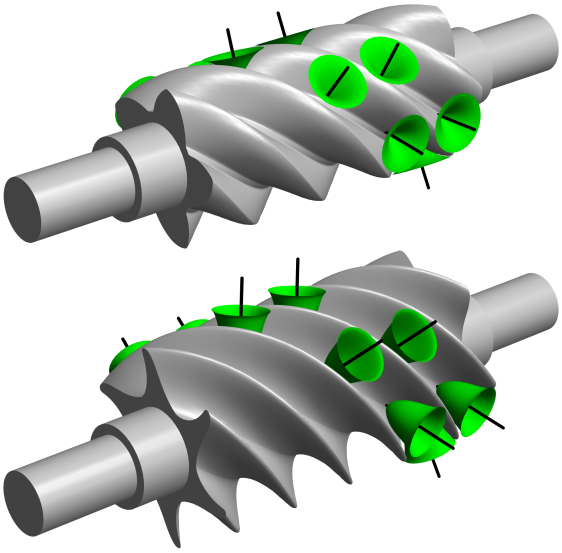

Figure 21: Approximate single-flank milling with one custom-shaped tool of male and female screw rotors ('N' profile, Stosic, 1996) from Example 4.9. Several positions of the custom-shaped tools are shown.

is then determined by the radial distance function $r(u)$ to X_1, see Figs. 18 and 19.

4.3. Single-flank milling with one custom-shaped tool

To further reduce the approximation error, we consider now the problem of milling of two helical surfaces of the screw rotor by the traditional (single-)flank milling, however, using a single custom-shaped tool. That is, we look for one tool and its two milling paths. This can be achieved as follows.

In particular, the tool is described by its radial function $r(t)$ and we seek two different starting positions given by the two axes o'_1 and o'_2. We recall that the position of o'_i is given by parameters $\alpha_i, \delta_i, \phi_i$, $i = 1, 2$, cf. (10).

Analogously to Section 4.2, we start with computing the foot points $\mathbf{b}_1^i$ and $\mathbf{b}_2^i$ of the points $\mathbf{a}_1^i$ and $\mathbf{a}_2^i$ sampled on the axes o'_1 and o'_2, respectively.

Then we define the objective function Φ as the maximum of the differences between the distances of the foot points $\mathbf{b}_1^i$, $\mathbf{b}_2^i$ and $\mathbf{a}_1^i$, $\mathbf{a}_2^i$, respectively

$$\Phi(\alpha_1, \delta_1, \phi_1, \alpha_2, \delta_2, \phi_2) = \max_{i=1,\dots,n} \left| \|\mathbf{b}_1^i - \mathbf{a}_1^i\| - \|\mathbf{b}_2^i - \mathbf{a}_2^i\| \right|. \tag{18}$$

For minimizing Φ the gradient descent method with finite differences can be effectively used.

Hence we obtain two positions of the tool T (axes o'_1 and o'_2) and two arrays of radii

$$r_1^i = \|\mathbf{b}_1^i - \mathbf{a}_1^i\|, \quad r_2^i = \|\mathbf{b}_2^i - \mathbf{a}_1^i\|, \qquad i = 1, \dots, n. \tag{19}$$

Finally, we construct the radial function of T by interpolating the values (14). The errors of the two approximate single-flank machining are given by (15).

We recall, that it generically happens (for asymmetric screw rotors), that the characteristics $\mathbf{c}_1$ and $\mathbf{c}_2$ are not of the equal length. Hence at some point we have to take care only of a part of one helical surface which leads to the exact single-flank milling of that part, see the red curves in Fig. 20.

Example 4.9 ('N' profile, Stosic, 1996 – single flank with one tool)**.** We again use the first guess the values $\mathbf{x}_0 = (\alpha_0^1, \delta_0^1, \phi_0^1, \alpha_0^2, \delta_0^2, \phi_0^2) = (0, 0, 0, 0, 0, 0)$. Both optimizations terminate after 11 iterations at $\mathbf{x} \doteq (-0.005, 0.191, 0.289, -0.008, 0.291, 0.189)$ for a male rotor and at $\mathbf{x} \doteq (-0.203, 0.006, 0.055, -0.203, 0.056, 0.015)$ for a female rotor, see Figs. 20 and 21. The maximal distances between the custom-shaped tool and the surfaces X_1 and X_2 corresponding to the male rotor are 0.00312 and 0.00315. For the female rotor we arrive at the distances 0.00573, 0.00575, see Fig. 22. Now comparing the maximal errors with the maximal errors from the double-flank approach, cf. Example 4.3, for the male and the female rotor we arrive at $0.00312 < 0.00362$ and $0.00575 < 0.01774$, respectively. We see that, for this specific rotors, the female part manufacturing can be considerably improved by considering single-flank variant with an adequate custom shaped tool, while the male gives almost the same error. We conclude that the male part is better suited for double-flank milling.

5. Double-flank milling by conical tools

In the previous sections we considered double-flank milling where the meridian of the tool was a general curve, an unknown in our optimization framework. However, it might be of more practical interest to consider double-flank milling – if possible by conical tools, i.e., tools with linear meridians. In this section we try to address this

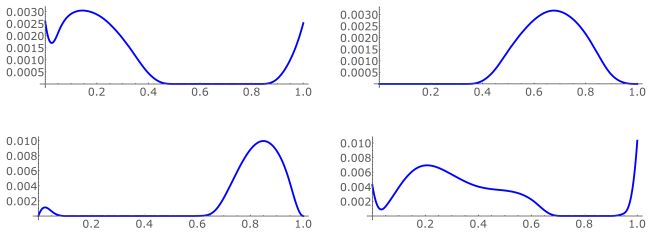

Figure 22: Error functions (15) (along the axis o') corresponding to radii (16) of the custom-shaped (male and female) tools and the helical surfaces X_1 (left) and X_2 (right) corresponding to the male (up) and female (bottom) rotors from Example 4.9.

issue as designing of custom-shape tools for rotors, with both symmetric and asymmetric profiles, leads to rather complicated tool meridians (radial functions). For a conical tool, the radial function is linear. In particular, for a given couple of helical surfaces X_1, X_2 we design a cone T (and its initial position) having the minimal maximum of distances from X_1 and X_2. Then by applying the helical motion to the cone T we double-flank machine the valley $X = X_1 \cup X_2$. It is expected that the linearity of the meridian will be paid by higher approximation error.

Analogously to Sections 4.2 and 4.3 the initial position of T will be obtained by minimizing the following objective function:

$$\Phi(\alpha,\delta,\phi) = \max_{i=1,\dots,n} \left|r_1^i - r_2^i\right| + \frac{1}{n-2}\left(\sum_{i=1}^{n-2}\left|r_1^i - 2r_1^{i+1} + r_1^{i+2}\right| + \sum_{i=1}^{n-2}\left|r_2^i - 2r_2^{i+1} + r_2^{i+2}\right|\right), \quad (20)$$

where radii r_1^i and r_2^i are given by (13). The objective function Φ is composed of three parts:

1. It measures the maximal difference between the radii r_1 and r_2, i.e., the difference between the distances of the axis o' and the helical surfaces X_1 and X_2, respectively;
2. It measures the second differences of the radii r_1;
3. It measures the second differences of the radii r_2;

Part 1. corresponds to the double-flank position of T whereas parts 2. and 3. are responsible for the linearity of the meridian of T.

Minimization of Φ yields the position (α,δ,ϕ) of T and the radii r_1^i and r_2^i. The final step is the determination the linear radial function $r(t) = a + b\,t$ fitting r_1^i and r_2^i. It simultaneously has to lie "bellow" r_1^i and r_2^i to ensure T does not penetrate X. The particular values a and b correspond to the minimum of the function

$$\Psi(a,b) = \sum_{i\in I_1} r_i - r(t_i) + w_2 \sum_{i\in I_2} r(t_i) - r_i, \quad (21)$$

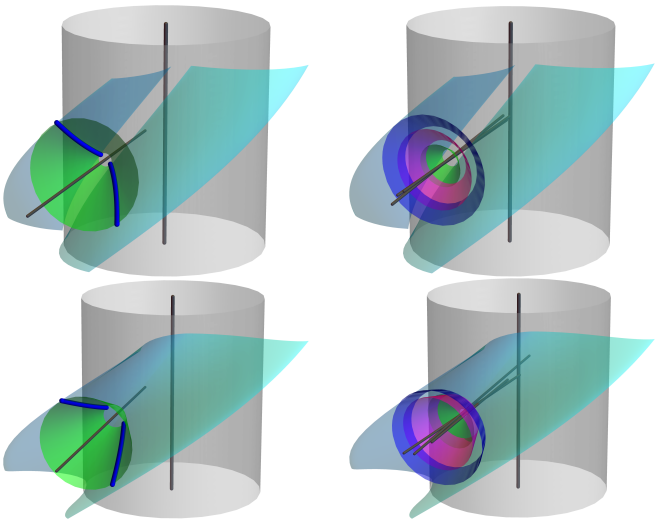

Figure 23: Double-flank machining of the helical surfaces of the male (top) and female (bottom) screw rotors by conical tools. Left: Only one tool is used. Right: Three different conical tools, where each tool focuses on different parts of X.

where $r_i > r(t_i)$ for $i \in I_1$ and $r_i < r(t_i)$ for $i \in I_2$. To penalize the parts with the over-cutting (I_2) we set the weight $w_2 = 100$.

Remark 5.1. Let us note, that we focused only on the parts of X where the double-flank milling can be achieved. However, this approach leaves a part of one of the helical surfaces, w.l.o.g. X_1, unmilled. Nonetheless, analogously to Sections 3 and 4, the approach can be adapted to provide a single-flank at the corresponding part of X_1.

Example 5.2 ('N' profile, Stosic, 1996 – conical tool)**.** We design the conical tools and its positions for male and female screw rotors with the 'N' profile. We again use as a first guess the values $\mathbf{x}_0 = (\alpha_0,\delta_0,\phi_0) = (0,0,0)$ and employ the optimization process. We arrive after 39 iterations at $(\alpha,\delta,\phi) \doteq (-0.025, 0.208, 0.21)$ for the male rotor and after 57 iterations at $(\alpha,\delta,\phi) \doteq (-0.054, 0.314, 0.272)$ for the female rotor. The radial functions of the conical tools are determined as $0.0871214 + 0.746243u$ and $0.134593 + 0.416458u$, $u \in [0,1]$ for the male and female rotor, respectively. The conical tools are shown in Fig. 23, left. In Fig. 24 several positions of the conical tools are shown. The maximum distances of the male tool and the surfaces X_1 and X_2 are 0.03439 and 0.03614, respectively. For the female rotor we obtain maximal errors 0.10488 and 0.10992, see Fig. 25.

We conclude that while the male rotor errors are on the edge of being practically applicable, the female rotor cannot be well-approximated by a screw motion of a conical tool.

Remark 5.3. The error can be improved by considering not one but several different conical tools such that each tool focuses on a different part of

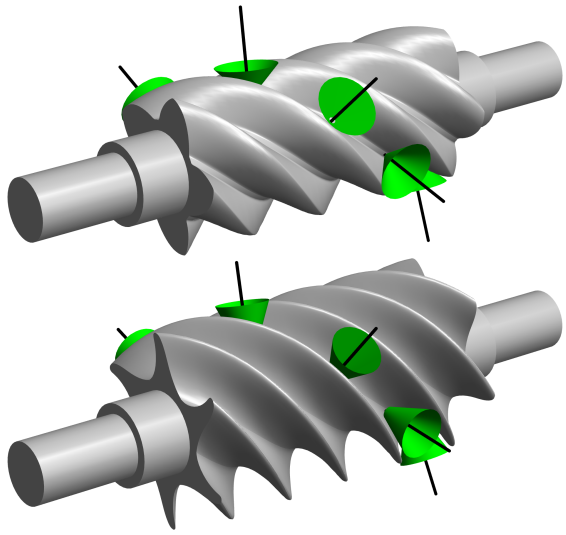

Figure 24: Approximate single-flank milling with one conical tool of male (up) and female (bottom) screw rotors ('N' profile, Stosic, 1996) from Example 5.2. Several positions of the conical tools are shown.

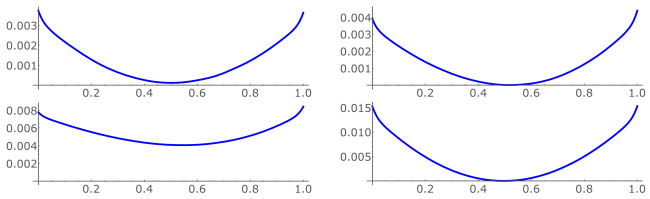

Figure 25: Error functions (15) (along the axis o') corresponding to the position of the conical tools and the helical surface X_1 (left) and X_2 (right) of the male (top) and female (bottom) screw rotors from Example 5.2.

X. In Fig. 23, right, three different conical tools (for male and female rotors) and their initial positions are shown. The maximal distances of the three male tools and the surfaces X_1 and X_2 are $0.003, 0.00357, 0.00374$ and $0.00693, 0.00578, 0.0044$, respectively. For the female rotor we arrive at $0.05223, 0.03572, 0.00841$ and $0.03406, 0.03528, 0.01531$.

The numerical experiments were all run on a standard laptop. The whole computation of each particular example took less than three seconds.

6. Conclusion

We have studied a problem of manufacturing of screw rotors using 5-axis double-flank milling. We have proven that for symmetric profiles, the double-flank milling is possible exactly, with a properly designed custom-shaped tool. For screw rotors with asymmetric profiles, we have presented an optimization-based framework and have shown empirically that the envelopes of custom-shaped tools approximate the input geometry with fine machining tolerances. We have validated our approach on several existing screw rotors.

Acknowledgment

The first author has been partially funded by the fellowship of the King Abdullah University of Science and Technology, KAUST-BRF grant nr. 3989 and the BCAM "Severo Ochoa" accreditation of excellence, Spain (SEV-2017-0718). The second author has been partially supported by Spanish Ministry of Science, Innovation and Universities: Ramón y Cajal with reference RYC-2017-22649, PID2019-104488RB-I00, and the European Union's Horizon 2020 research and innovation programme under agreement No. 862025.

References

[1] P. Bo, H. González, A. Calleja, L. N. L. de Lacalle, M. Bartoň, 5-axis double-flank CNC machining of spiral bevel gears via custom-shaped milling tools—part I: Modeling and simulation, Precision Engineering 62 (2020) 204–212.

[2] N. Stosic, I. Smith, A. Kovacevic, Screw Compressors: Mathematical Modelling and Performance Calculation, Springer Berlin Heidelberg, 2005.

[3] A. Kovacevic, N. Stosic, I. K. Smith, Advanced methods and tools for screw compressor design, Proceedings of the TMCE 2006 (2006).

[4] N. Stosic, I. K. Smith, A. Kovacevic, E. Mujic, Geometry of screw compressor rotors and their tools, Journal of Zhejiang University-SCIENCE A 12 (4) (2011) 310–326.

[5] F. L. Litvin, P.-H. Feng, Computerized design, generation, and simulation of meshing of rotors of screw compressor, Mechanism and Machine Theory 32 (2) (1997) 137–160.

[6] F. L. Litvin, A. Fuentes, Gear geometry and applied theory, Cambridge University Press, 2004.

[7] J. Machchhar, H. Segerman, G. Elber, Conjugate shape simplification via precise algebraic planar sweeps toward gear design, Computers & Graphics (2020).

[8] H. Xu, T. Fu, P. Song, M. Zhou, N. Mitra, F. Chi-Wing, Computational design and optimization of non-circular gears, Computer Graphics Forum (2020).

[9] X. He, C. Pan, M. Wu, X. Ji, R. Zhang, A twin-screw rotor profile design and computational fluid dynamic simulation method, Materials Research Innovations 19 (sup8) (2015) S8–721.

[10] S. Cao, X. He, R. Zhang, J. Xiao, G. Shi, Study on the reverse design of screw rotor profiles based on a b-spline curve, Advances in Mechanical Engineering 11 (10) (2019) 1687814019883782.

[11] W. Wunderlich, Geometrische Grundlagen für das Fräsen von Schraubnuten I, Österr. Ing. Arch. VI S (1952) 315–326.

[12] W. Krumme, Klingelnberg–Spiralkegdräder (Klingelnberg Spiral Bevel Gears) (in German), Springer, 1967.

[13] H. J. Stadtfeld, Gleason Bevel Gear Technology: The Science of Gear Engineering and Modern Manufacturing Methods for Angular Transmissions, Gleason Works, 2014.

[14] L. Rinder, Screw rotor profile and method for generating, uS Patent 4,643,654 (1987).

[15] J. Do Suh, D. G. Lee, Manufacture of composite screw rotors for air compressors by rtm process, Journal of Materials Processing Technology 113 (1-3) (2001) 196–201.

[16] S. Flöry, H. Pottmann, Ruled surfaces for rationalization and design in architecture, in: LIFE in:formation. On Responsive Information and Variations in Architecture, 2010, pp. 103–109.

[17] M. Bartoň, H. Pottmann, J. Wallner, Detection and reconstruction of freeform sweeps, Computer Graphics Forum 33 (2) (2014) 23–32.

[18] P. Bo, H. Pottmann, M. Kilian, W. Wang, J. Wallner, Circular arc structures, ACM Trans. Graph. 30 (4) (2011) 101.
[19] M. Bartoň, L. Shi, H. Pottmann, M. Kilian, J. Wallner, Circular arc snakes and kinematic surface generation, Computer Graphics Forum 32 (1) (2013) 1–10.
[20] M. Bizzarri, M. Lávička, J. Kosinka, Skinning and blending with rational envelope surfaces, Computer-Aided Design 87 (2017) 41 – 51.
[21] Y.-J. Kim, Y.-T. Oh, S.-H. Yoon, M.-S. Kim, G. Elber, Efficient hausdorff distance computation for freeform geometric models in close proximity, Computer-Aided Design 45 (2) (2013) 270 – 276, solid and Physical Modeling 2012.